Research Article Vol. 2, No. 2 / 15 Feb 2023 / Optics Continuum 327
OPTICS CONTINUUM

Simultaneous measurements of forward Thomson scattering and rotational Raman scattering in a weakly ionized plasma

ZICHEN HE,[1] RAJAGOPALAN V. RANGANATHAN,[1] D. T. FROEDGE,[2] AND ZHILI ZHANG[1,*]

[1]Mechanical, Aerospace and Biomedical Engineering, University of Tennessee-Knoxville, Knoxville, TN 37996, USA
[2]Geosonics Vibra-tech, 9117 Leesgate Road, Louisville, KY 40223, USA
*zzhang24@utk.edu

Abstract: This paper demonstrates a simultaneous Thomson scattering and rotational Raman scattering spectroscopy in a weakly ionized plasma in air. Thomson scattering was collected in the forward scattering direction, in order to compress the relative spectra width of Thomson scattering from the plasma. Simultaneous measurements of rotational Raman scattering were obtained in the same direction, which was not affected by the collection angles. The measurements thus yielded electron temperature (T_e) and electron number density (n_e) as well as gas temperature in a weakly ionized atmospheric pressure plasma. The separation of rotational Raman scattering and Thomson scattering occurred when the scattering angle decreased to 20 degrees in the plasma, where the air temperature was found to be 150 ± 25 °C, and electron temperature of the plasma was 0.587 ± 0.087 eV, and electron number density was (1.608 ± 0.416) × 1021 m-3. The technique could be used for various plasma and combustion diagnostics in realistic engineering environments.

1. Introduction

It is essential to study the characteristics of atmospheric pressure plasma (APP) due to its increasing applications in industries such as medicine [1], adhesives [2], catalysis [3], and food processing [4]. In a weakly ionized plasma, the vast difference in temperatures between electrons and neutrals results in using APP for heat-sensitive materials like food [5] and skin [6]. The measurements of electron number density and temperature [7] are vital due to its interaction with various species, which enhances the physicochemical properties of plasma and its interactions with the exposed surface. The creation of reactive molecular species [8] is dependent on direct electron impact reactions, such as dissociation and excitation of the molecules. Electron kinetics play a significant role in these reactions, and it is directly related to electron temperature. Thus, measuring the electron number density and temperatures is salient in studying various plasma parameters for creating new plasma reactors that will have enhanced and reliable performance with longer lifetimes.

Laser Thomson scattering (TS) diagnostics has been demonstrated as a reliable and well-trusted plasma diagnostic technique for electron temperature (T_e) and electron number density (n_e) measurements [9–11]. However, in plasmas made of molecular species at moderate pressures (>10 Torr) at low electron temperature (T_e ~ 1-10 eV), the rotational Raman scattering (RR) can be overlapped with the TS spectrum. For instance, in a TS measurement of a weakly ionized plasma, RR emission is also captured in the spectrum [8,12,13]. Also, in hypersonic flows [14], where the electron number density is relatively low compared to the neutral number density, RR interferes directly with TS. Conventionally, separating RR spectrum from TS spectrum requires subtracting a fitted RR spectrum [13]. This is only reliable when the temperature of the gas

#474339 https://doi.org/10.1364/OPTCON.474339
Journal © 2023 Received 31 Aug 2022; revised 26 Dec 2022; accepted 1 Jan 2023; published 27 Jan 2023

OPTICS CONTINUUM

is already known, so a theoretical RR spectrum can be determined and subtracted from the overlapped "RR + TS" spectra. For cases where gas temperature is unknown or hard to determine, such as in a weakly ionized plasma with gas being heated by the plasma, the RR spectrum cannot be determined without making an assumption or estimation of the gas temperature, which makes the Raman-subtraction-based RR-TS separation unreliable, especially in cases where the plasma conditions and gas temperature is time-variant.

An alternative approach, whether the temperature of the gas is known or not, is to separate RR and TS physically, by utilizing forward collection angles [14]. Previously, Filip et al. applied forward Thomson scattering [15] for the detection of relativistic waves in plasma density of $2\,10^{15}\,\mathrm{cm}^{-3}$. Also, Glenzer et al. used forward TS for measuring high-density plasmas using X-ray [16]. Forward TS is obtained by placing the collection optics in a forward direction, i.e., the angle of the Thomson scattering collected by the imaging system is smaller than 90 degrees. As TS is essentially an elastic collision between photons from the incident laser and the free electrons in the plasma, the frequency of the scattered photons is unchanged. However, from the observer's view, the frequency of the Thomson scattered photons are shifted due to the Doppler shift, as illustrated in Eq. (1),

$$\Delta\lambda = \lambda_s - \lambda = (\boldsymbol{k} \cdot \boldsymbol{v})\,\lambda^2 / (2\pi c) \tag{1}$$

where λ_s is the observed wavelength of the scattered photons, and λ is the wavelength of incident photons, vector $\boldsymbol{k}$ denotes the differential scattering wave factor, and $\boldsymbol{v}$ and c are the velocity of electron and the speed of light, respectively. As discussed in [17], the Thomson scattering has a Gaussian profile due to Doppler broadening effects. The full width at half maximum (FWHM) of the Gaussian curve is used to determine the electron temperature (T_e) of the plasma, as illustrated in Eq. (2) [18,19]. Moreover, the scattering angle is also a factor in the T_e calculation, as indicated in Eq. (2),

$$T_e = \frac{m_e c^2}{8k_B \sin^2(\theta/2)} \times \frac{\Delta\lambda^2}{\ln(2)\lambda^2} \tag{2}$$

where m_e is the electron mass, k_B is the Boltzmann's constant, θ is the scattering angle, and $\Delta\lambda$ is the half width at half maximum of the TS profile. The n_e is calibrated with rotational Raman spectrum of nitrogen in air, as shown in Eq. (3) [18,19],

$$n_e = \frac{A_e}{A_{N_2}} \times \frac{d\sigma_{N_2}/d\Omega}{d\sigma_e/d\Omega} \times n_{N_2} \times f \tag{3}$$

where A_e is the total emission power of TS, A_{N_2} is the total emission power of RR line of nitrogen at $J = 4 \rightarrow 6$, $d\sigma_{N_2}/d\Omega$ and $d\sigma_e/d\Omega$ are differential cross section of RR of nitrogen at 532 nm and differential cross section of TS, respectively, n_{N_2} is the molecule number density of nitrogen in air, and lastly, f is the fraction of RR of nitrogen at $J = 4 \rightarrow 6$ transition.

The uncertainty of measuring T_e and n_e with TS diagnostics is respectively defined by Eqs. (4) and (5) [18],

$$\delta T_e = \frac{m_e c^2}{8k_B \sin^2(\theta/2)} \times \frac{\delta\Delta\lambda^2}{\ln(2)\lambda^2} \tag{4}$$

$$\delta n_e = \frac{\delta A_e}{A_{N_2}} \times \frac{d\sigma_{N_2}/d\Omega}{d\sigma_e/d\Omega} \times n_{N_2} \times f \tag{5}$$

where δT_e and δn_e are respectively the statistical uncertainty of T_e and n_e, $\delta\Delta\lambda$ and δA_e are respectively the uncertainty of fitted HWHM of TS spectrum and integrated intensity of TS.

Therefore, for a plasma with a constant T_e, the measured HWHM of its TS profile becomes smaller as the scattering angle of collected the Thomson scattered photons becomes smaller. On the other side, as the RR emission is associated with energy released from laser-excited

OPTICS CONTINUUM

polyatomic molecules returning from a higher (virtual) energy level to lower ones, and the energy levels are independent of scattering angle, the wavelengths of RR emission do not change with scattering angles [20]. Therefore, it is possible to separate TS and RR spectrum by narrowing the TS spectrum by detecting TS in a forward direction [14] so that TS stays in the gap between the Stokes and anti-Stokes lines of RR. Figure 1 shows that theoretical forward TS spectrum of a plasma with constant T_e and n_e becomes narrower than the TS spectrum obtained from 90-degree scattering. The benefit of this technique not only separates TS and RR spectra but also allows simultaneous measurements of electron temperature and electron number density of the plasma via TS and the temperature of the gas via RR.

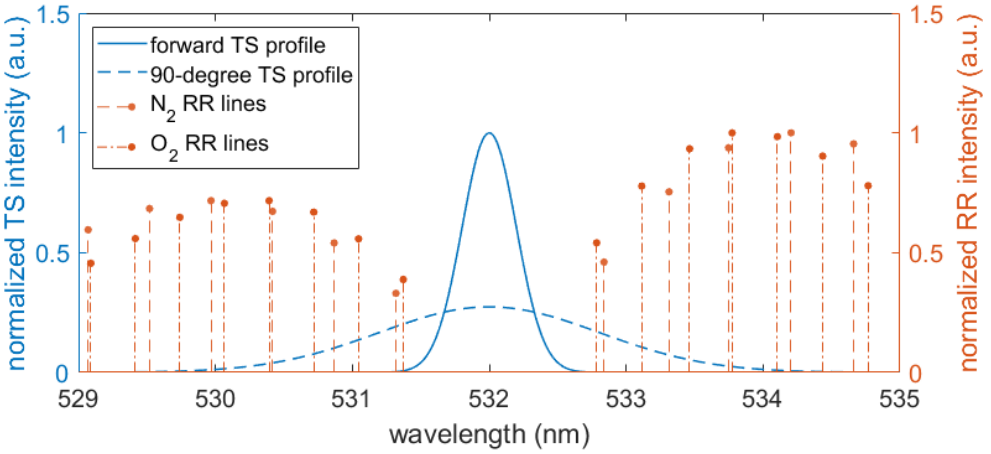

Fig. 1. Theoretical forward TS spectrum of a plasma with constant T_e and n_e becomes spectrally narrower than the TS spectrum obtained at 90 degree, thus "sits" between the gap between the Stokes and anti-Stokes lines of RR spectrum of air. Thus RR and TS are spectrally separated. TS spectra are normalized to the height of the forward TS spectrum, RR lines are normalized to its highest line.

Here the simultaneous measurements of TS and RR from a weakly ionized atmospheric pressure plasma and plasma-heated air were demonstrated by using forward collection angles. Electron temperature and electron number density of the plasma, as well as the air temperature were determined simultaneously. The parameters measured will be useful in validating or improving the computational simulation of atmospheric pressure plasmas.

2. Experimental design

2.1. Plasma source

The atmospheric pressure plasma was a pin-to-pin glow discharge of weakly ionzied air (nonthermal plasma, scattering parameter α was 0.4 degrees scattering) with a tip-to-tip electrode distance of 0.5 inch. It was powered by a high-power AC source (CTP-2000K, Nanjing Suman Plasma Technology Co., Ltd.) with an adjustable input voltage set on 260 Volt AC, and an input current at 260 mA. And the output voltage of the source was 30 kVAC with an adjustable output frequency set on 22 kHz, the output current was estimated to be a few mA. The full set of the power source consists of the high-power AC power source and two transformers (120 V to 220 V). The output of power source is controlled by the adjustable voltage transformer.

OPTICS CONTINUUM

2.2. Thomson scattering setup

TS spectra are taken from scattering angles of 20, 30, 50, 70 and 90 degrees while the plasma remains the same. RR spectra of ambient air (not heated by plasma) from each angle are also separately obtained for corresponding n_e calibrations as well as system alignment verification [10]. The TS setup for 90 degrees scattering is illustrated in Fig. 2(a). The probing laser was a Nd: YAG pulsed laser (Powerlite 8020) running on 10 Hz mode (outputs 120 mJ/pulse at 532

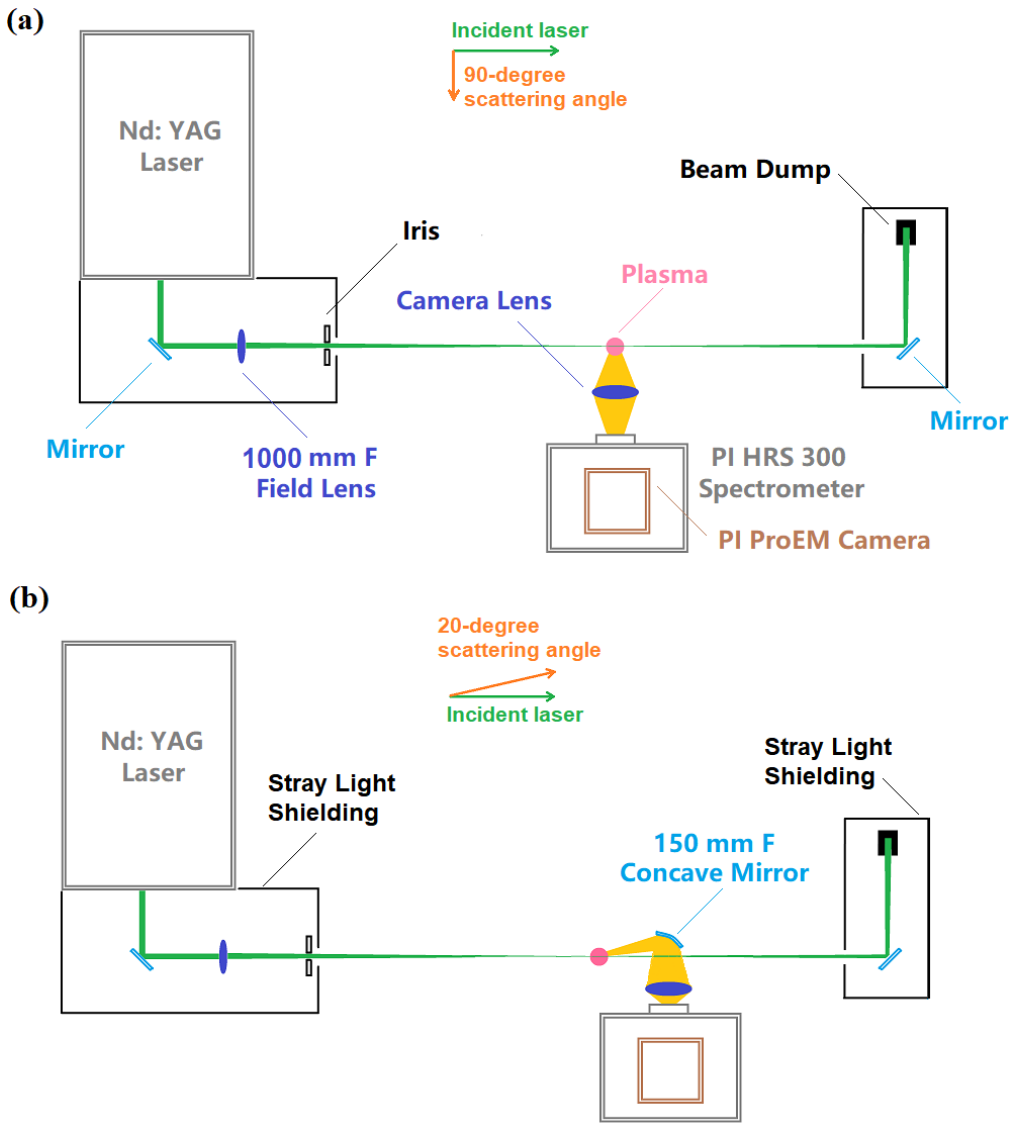

Fig. 2. (a) Diagram of the 90-degree Thomson scattering setup from a top-down view. For 30 to 70 degrees scattering, the camera lens and the imaging system were moved accordingly to the corresponding forward positions to collect 20-, 30-, 50-, 70-degree Thomson scattering spectra. (b) Diagram for 20-degree forward Thomson scattering. Due to the sharp angle, an additional concave mirror was placed at the 20-degree position to collect Thomson scattered photons.

OPTICS CONTINUUM

nm, pulse width 7 ns). The laser was first focused by a field lens with a 1000 mm focal length to generate intensity $\sim 1.1 \times 10^{10}$ W/cm^2. The focused laser probed the plasma that was generated between the electrodes. Finally, the laser was collected by a beam dump. The Thomson scattering photons were collected by a camera lens (focal length 50 mm). And the imaging system consisting of a spectrometer (Princeton Instrument SpectraPro HRS-300) and an electron-multiplying CCD camera (Princeton Instrument ProEM HS) was used to obtain the 90-degree TS spectrum. For 30- to 70- degree scattering, the camera lens and the imaging system were moved accordingly to the corresponding forward positions to collect those forward TS spectra. The TS setup for 20 degrees scattering was different from the others, because the angle was too sharp to just move the camera lens and the imaging system. Therefore, an additional concave mirror of 150 mm focal length was placed at the 20-degree position to reflect the forward Thomson scattered photons into the camera lens, as shown in Fig. 2(b).

2.3. *Stray light removal*

Since TS is weak compared to incident laser beam, it is crucial to reduce the background and stray light to increase the signal-to-noise ratio of the TS spectrum. Stray light mostly comes from the reflections of the laser optics, and secondary reflections from other surfaces in the proximity. As the plasma was generated in atmospheric air, there was no vacuum chamber to obtain a stray light profile that can be directly subtracted from the TS spectrum in the post-processing. Therefore, a stray light mitigation setup was implemented to physically reduce the stray light intensity to near zero. As shown in Fig. 2, multiple laser safety screens were used to form two housings to contain the laser optics inside, so that all the reflections from the optics were boxed in, hence removing stray light. Figure 3(a) and (b) compare the intensity of stray light "before" and "after" the stray light mitigation. Figure 3(c) shows an image of the laser beam intercepting the center of the atmospheric pressure plasma after the stray light mitigation was in place.

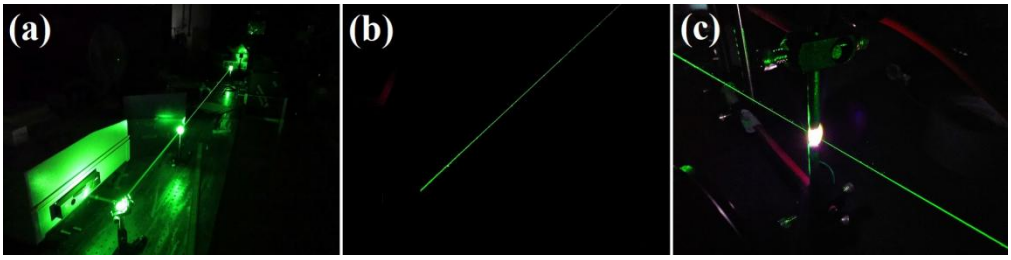

Fig. 3. Demonstration of stray light mitigation for atmospheric pressure plasma. (a) An image of the laser beam and stray light before the stray light mitigation. (b) An image of the laser beam taken with the same camera settings after the mitigation process. The stray light intensity had been reduced to near zero. (c) An image of the laser beam probing the center of atmospheric pressure plasma after the stray light mitigation was in place.

3. Experiment results

RR spectra of ambient air from various forward scattering angles were first conducted as system alignment checks, and the Stokes line at transition $J = 4 \rightarrow 6$ from each scattering angle was used with corresponding forward TS spectrum to calibrate the electron number density of n_e in the plasma. Figure 4 shows the RR spectrum obtained at 90 degrees (averaged over 300 shots) as an example, the red and blue dashed lines indicate the wavelengths and intensities of theoretical RR lines of N_2 and O_2, respectively, which is a good match with the experimental data. Subsequently, TS spectra at scattering angles of 90, 70, 50, 30 and 20 degrees were obtained while the plasma maintained the same (same electrode distance and same output power from the plasma source).

OPTICS CONTINUUM

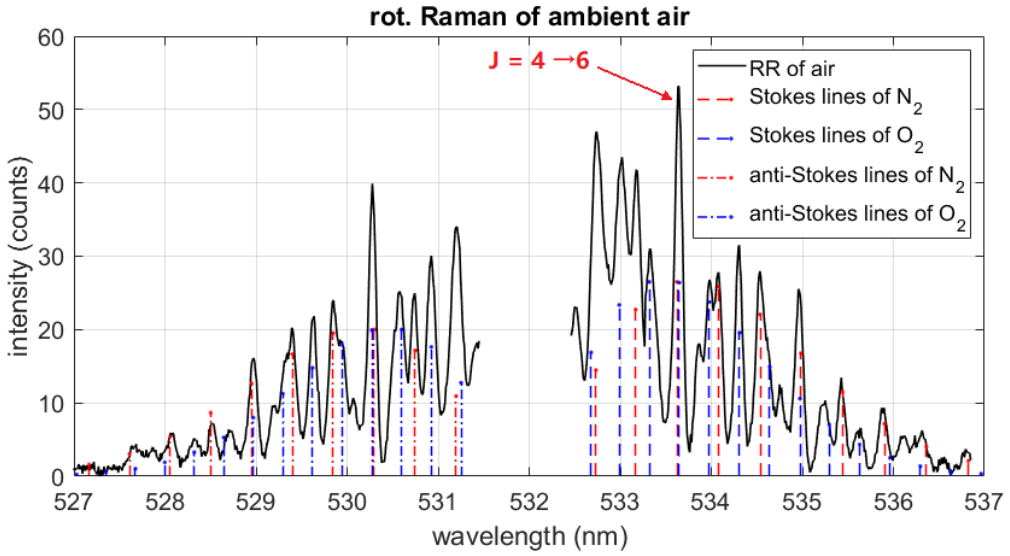

Fig. 4. Rotational Raman spectrum of ambient air obtained at 90-degree scattering angle. The red and blue dashed lines indicate the wavelengths and intensities of theoretically rotational Raman lines of N_2 and O_2, respectively.

Figure 5 shows TS spectra obtained from the plasma at 90- and 20-degree scattering angles as the best examples: TS spectrum being entangled with RR spectrum at 90 degrees and TS spectrum being separated from RR spectrum in the forward 20-degree direction. From 90 to 20 degrees, each spectrum was an average of 300 shots. For spectra from 90 to 30 degrees, the T_e was hot enough for the TS spectrum to expand into the RR spectral region. Therefore, for spectra from 90 to 30 degrees, TS and RR were separated by subtracting a theoretical RR spectrum based on the assumption that the air temperature was at room temperature (22 °C). But as the scattering angle decreased, the FWHM of the TS profile was reduced. When the scattering angle came down to 20 degrees, the TS spectrum became narrow enough to "sit" within the gap between the RR Stokes lines and anti-Stokes lines, thus achieving RR-TS separation in the forward scattering direction. It should be noted that the TS spectral profile was obtained by fitting a Gaussian curve based on the "wings" of the TS spectrum, as the central part (532 nm) is dominated by Rayleigh scattering in Fig. 6.

It is now possible to determine the air temperature from the RR spectrum by finding the best fit via adjusting the temperature parameter of a theoretical RR spectrum to the RR portion of the data, since the RR spectrum does not interfere with the TS spectrum in the 20-degree forward scattering. As shown in Fig. 6, a simulated RR spectrum is fitted to the RR section of the 20-degree forward "RR + TS" scattering data. The broadening in the simulated Raman lines is based on the instrument broadening (slit width of the spectrometer), which is the major source of the broadening effect for RR. The fitting of the RR lines suggests the air temperature in the plasma was 150 ± 25 °C.

Figure 7(a) displays the fitted TS profiles obtained from the same atmospheric pressure plasma from all the scattering angles and theoretical RR lines at 150 °C. For this particular plasma, the bottom part of the TS from 20-degree scattering was wide enough to fit in the "gap" between the Stokes and anti-Stokes lines of RR. Figure 7(b) and (c) respectively show T_e and n_e of the plasma calculated from all the TS spectra. From 90 to 30 degrees, TS profile was obtained by subtracting a theoretical RR spectrum from the RR + TS spectra, while the gas temperature was assumed to be room temperature, only at 20 degrees scattering angle, the RR-TS separation occurred, and

OPTICS CONTINUUM

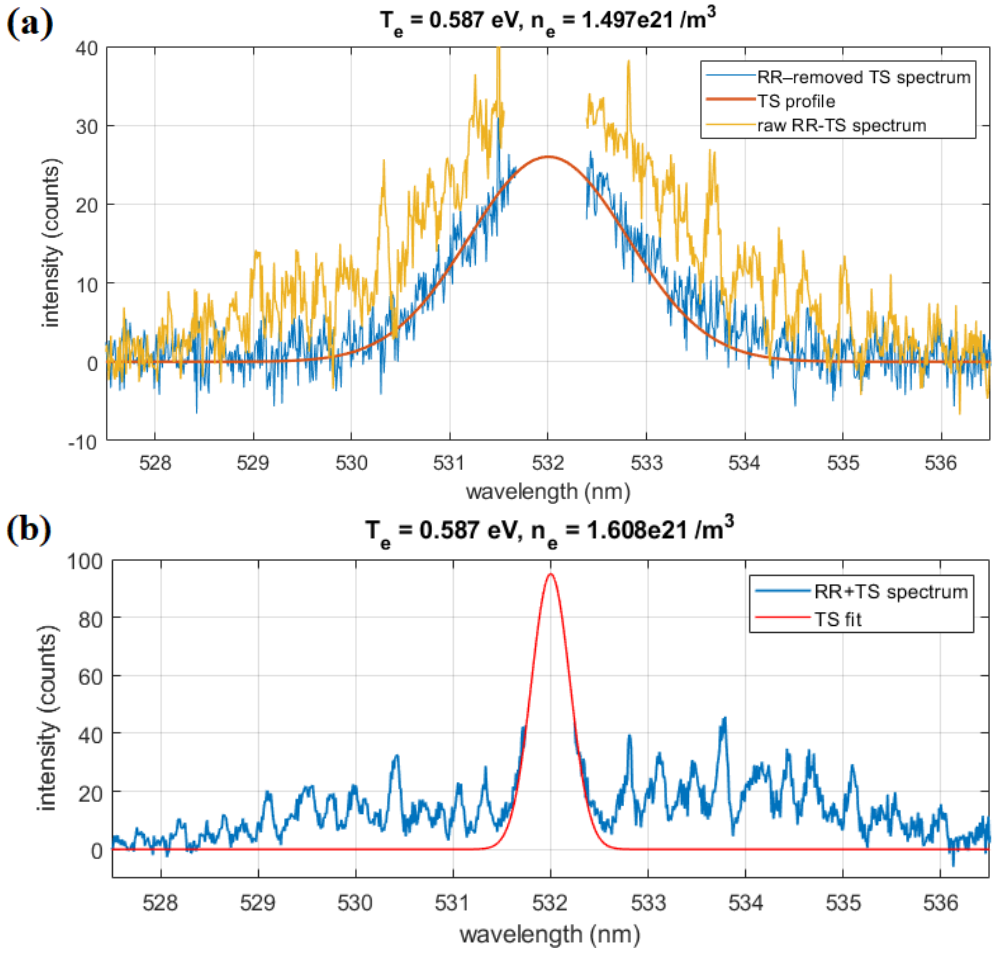

Fig. 5. (a) From 90 degrees scattering angle, the "wings" of Thomson scattering expanded into the lines of rotational Raman of air, becoming a baseline offset for RR. (b) At 20 degrees, TS spectrum becomes narrow enough to be separated from rotational Raman scattering.

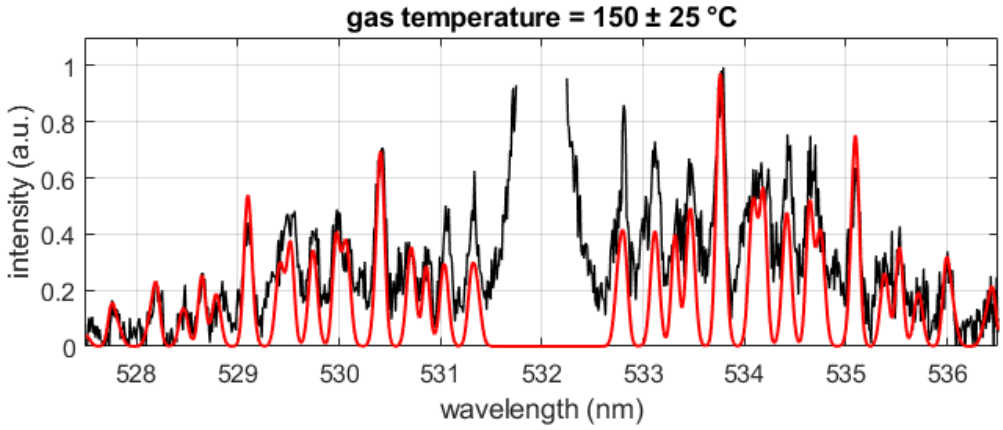

Fig. 6. A simulated RR spectrum is fitted to the normalized RR portion of the 20-degree forward RR-TS scattering data. The spectrum was normalized to its strongest RR line. The fitting of the RR lines suggests the air temperature was 150 ± 25 °C.

OPTICS CONTINUUM

gas temperature was directly obtained from finding the best RR fit to the RR spectrum. From 20 to 90 degrees, the T_e are respectively 0.587 ± 0.087, 0.575 ± 0.062, 0.585 ± 0.035, 0.581 ± 0.039, and 0.587 ± 0.063 eV; and the n_e are respectively $(1.608 \pm 0.416) \times 10^{21}$, $(1.531 \pm 0.325) \times 10^{21}$, $(1.566 \pm 0.371) \times 10^{21}$, $(1.582 \pm 0.369) \times 10^{21}$, and $(1.497 \pm 0.393) \times 10^{21}$ m^{-3}. Both T_e and n_e are fairly consistent throughout the measurements at all the scattering angles. The errors of the

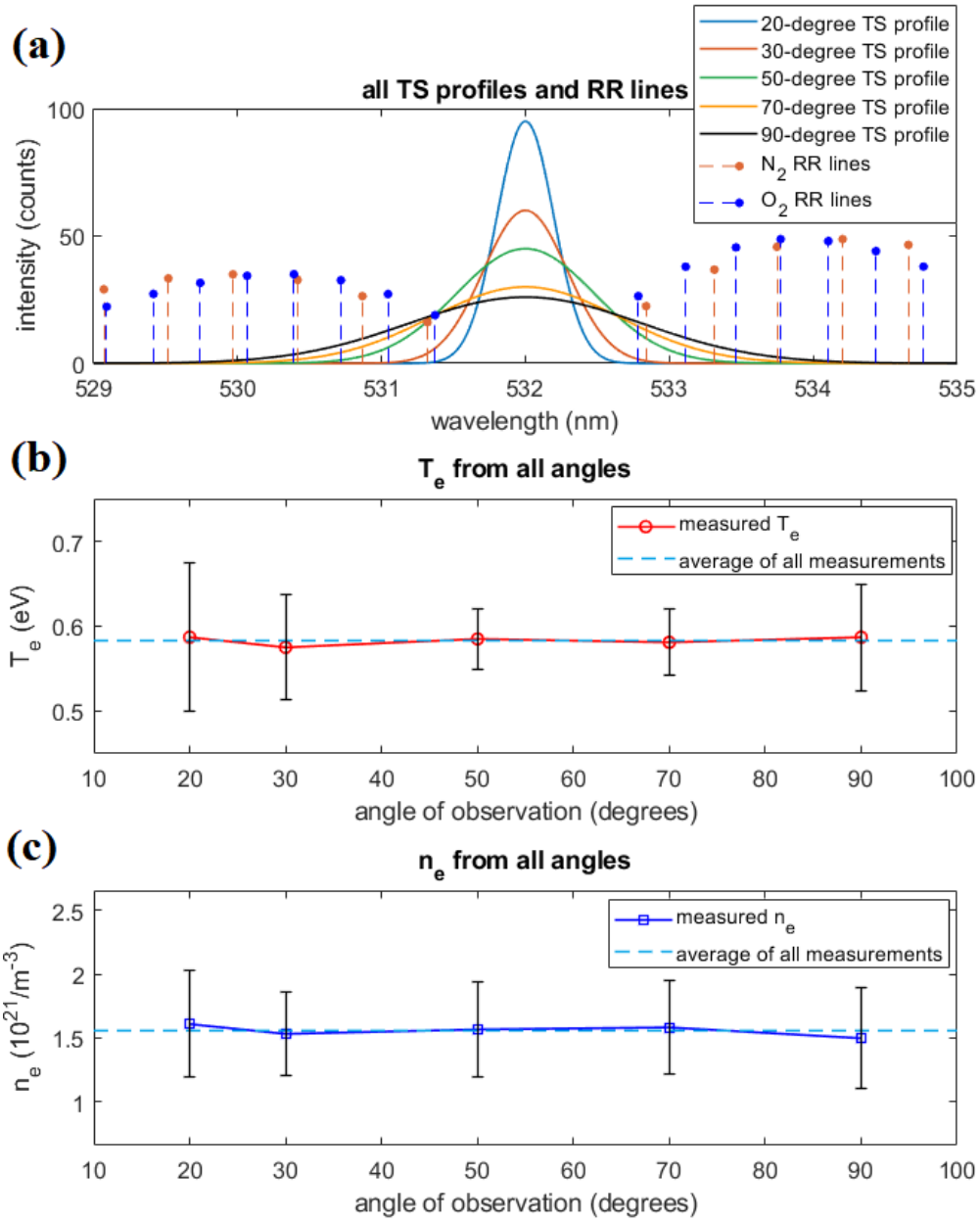

Fig. 7. (a) TS profiles fitted from TS spectra with scattering angle 20, 30, 50, 70 and 90 degrees, as well as theoretical rotational Raman lines of air. (b) T_e calculated from the Thomson scattering spectra. (c) n_e calculated from the Thomson scattering spectra.

OPTICS CONTINUUM

measured electron temperatures and densities are propagated through the statistical uncertainty of the instruments and fitting errors.

4. Discussions

The immediate and the most important benefit of forward TS is the spectral separation of RR and TS. From Fig. 8(c), T_e and n_e obtained from the conventional RR-subtraction technique is about the same as forward TS technique within the range of error bars. However, forward TS eliminates the necessity of making an assumption of the gas temperature, and instead, it allows direct measurement of gas temperature from the RR + TS spectrum. Additionally, imaging from a forward position is able to increase the SNR. Because for the same plasma, while its FWHM decreases with the scattering angle, its n_e maintains the same. As n_e is proportional to the total emission power of TS, the amplitude of the narrowed TS profile increases to maintain the area (total emission power) of the TS Gaussian profile, thus increasing TS signal strength, and SNR.

The disadvantage of forward TS technique is that the Rayleigh scattering (RS) and stray light contamination overlap on the TS spectrum more than conventional 90-degree TS scattering (RS contamination could be reduced with a phyiscal or an optical notch filter). As the TS spectrum narrows, more of the TS spectrum "merges" into the RS band (due to broadening, which is a very narrow band centered on incident laser wavelength) and the "wings" of TS becomes smaller and harder to identify. And this could potentially increase the fitting error, but the benefit of better SNR from forward scattering also helps with the curve fitting and reduces the fitting error.

Another disadvantage of forward TS is possible negative impact on the accuracy of TS measurement. According to Eq. 2, the electron temperature of T_e is proportional to $\Delta\lambda^2/\sin^2(\theta/2)$, where $\Delta\lambda$ is the FWHM of the TS profile and θ is the scattering angle. As the scattering angle θ approaches 0 degree, the slightest change of FWHM of TS profile would result in a large change of T_e fitting. The increase of fitting error for TS profile not only comes from the difficulty of fitting the smaller TS "wings", but also the increased T_e's sensitivity to scattering angles ($\sim$2% fitting error for 90-degree scattering, and $\sim$10% for 20-degree scattering due to T_e's sensitivity to scattering angle). Another notable point for scattering angle is that the Salpeter scattering parameter α also changes with scattering angle. In this experiment, the plasma maintained the same, but α increased from 0.4 to 1.69 due to change of scattering angle (from 90 degrees to 20 degrees). So, an incoherent TS could shift into coherent domain if observed from a small scattering angle, and the spectral shape of TS spectrum as well as the calculation of T_e could change, especially for high intensity lasers. So, a "soft limit" for scattering angle is that the angle must not be too small that TS becomes coherent, nor the uncertainty of fitting becomes too large that the fitted result becomes unconvincing (e.g. the fitting error goes up to $\sim$100% for incoherent TS at 2-degree scattering).

Overall, forward TS has a benefit of higher SNR in the TS spectrum which reduces fitting error, but it also suffers from the difficulty of fitting due to smaller TS "wings" and increased T_e's sensitivity to scattering angle, which both increase the fitting error. Whereas 90-degree TS does not have a SNR boost, it does not suffer from increased uncertainty of fitting either, as T_e is less "sensitive" to scattering angle, and the spectrum is less affected by RS (though it overlaps with RR instead). This could be the reason that the error bars of T_e are bigger at 20 and 90 degrees in Fig. 7(b), but smaller in the middle. The relative large error bar at 20 degrees is mostly the contribution of T_e becoming sensitive to scattering angle, and at 90 degrees it's mostly contributed by the noise (relatively lower SNR) in the spectrum, whereas TS at 50 degrees is a balance between SNR and T_e 's sensitivity to scattering angle, and resulted in the smallest error bar.

On the other hand, there is not a hard limit for maximum FWHM in forward TS technique either. As mentioned above, RS and stray light contaminates TS spectrum, and as TS gets

OPTICS CONTINUUM

narrower, the smaller the "wings" of TS will be left to identify the TS profile and the harder it is to fit it, so the wider the TS spectrum, the easier it is to identify its profile. But, to accommodate spectral separation, the TS spectrum can only be as wide as the "gap" between the Stokes and anti-Stokes lines of RR, which puts a limit to FWHM as well. Since the "gap" varies with the composition of the gas, the maximum allowed FWHM, instead of being a constant, changes with the RR spectrum.

5. Conclusions

Thomson scattering is an important optical diagnostics tool to measure electron number density and electron temperature in plasmas. A forward scattering-based RR-TS separation technique has been demonstrated to separate a RR and TS spectrum simultaneously obtained from a weakly ionized atmospheric plasma while the gas was heated to a certain temperature by the plasma. This technique allows simultaneous measurements of gas temperature, electron number density, and electron temperature of the weakly ionized plasma without the necessity of assuming the gas temperature. "RR + TS" spectra were obtained at 90, 70, 50, 30, and 20 degrees, and for this particular plasma, the complete RR-TS separation occurred as the scattering angle decreased to 20 degrees. Based on the 20-degree forward scattering, the air temperature was found to be 150 ± 25 °C, via fitting the RR spectrum; and electron temperature of the plasma calculated from the 20-degree Thomson scattering spectrum was 0.587 ± 0.087 eV, and electron number density was $(1.608 \pm 0.416) \times 10^{21}$ m^{-3}.

While forward TS may suffer from increased fitting error, it increases the SNR and lowers the detection limit of n_e, for this TS system, the detection limit of n_e is 1.641×10^{19} m^{-3}. And the RR-TS separation is limited by the gas type, as the "gap" between the RR Stokes and anti-Stokes lines varies with RR spectrum of different gases. In the future, this methodology can be applied to atmospheric plasmas, plasma biomedicine, plasma catalysis, surface adhesion, and food processing. The measured data will help simulate plasma for understanding the reaction mechanism resulting in the evolution of species of interests.

Funding. U.S. Department of Energy (DE-SC0021382); National Science Foundation (2026242).

Acknowledgment. We would like to recognize the suggestions from Dr. Theodore Biewer in the error analysis.

Disclosures. The authors declare no conflicts of interest.

Data Availability. The data that support the findings of this study are available from the corresponding author upon reasonable request.

References

1. M. Laroussi, "Cold Plasma in Medicine and Healthcare: The New Frontier in Low Temperature Plasma Applications," Front. Phys. **8**, 74 (2020).
2. M. Kehrer, A. Rottensteiner, W. Hartl, J. Duchoslav, S. Thomas, and D. Stifter, "Cold atmospheric pressure plasma treatment for adhesion improvement on polypropylene surfaces," Surf. Coat. Technol. **403**, 126389 (2020).
3. A. Bogaerts, X. Tu, J. C. Whitehead, G. Centi, L. Lefferts, O. Guaitella, F. Azzolina-Jury, H.-H. Kim, A. B. Murphy, W. F. Schneider, T. Nozaki, J. C. Hicks, A. Rousseau, F. Thevenet, A. Khacef, and M. Carreon, "The 2020 plasma catalysis roadmap," J. Phys. D: Appl. Phys. **53**(44), 443001 (2020).
4. D. A. Laroque, S. T. Seó, G. A. Valencia, J. B. Laurindo, and B. A. M. Carciofi, "Cold plasma in food processing: Design, mechanisms, and application," J. Food Eng. **312**, 110748 (2022).
5. S. K. Pankaj, Z. Wan, and K. M. Keener, "Effects of Cold Plasma on Food Quality: A Review," Foods **7**(1), 4 (2018).
6. M. A. Bogle, K. A. Arndt, and J. S. Dover, "Evaluation of Plasma Skin Regeneration Technology in Low-Energy Full-Facial Rejuvenation," Arch. Dermatol. **143**(2), 168–174 (2007).
7. R. Engeln, B. Klarenaar, and O. Guaitella, "Foundations of optical diagnostics in low-temperature plasmas," Plasma Sources Sci. Technol. **29**(6), 063001 (2020).
8. S. Park, W. Choe, S. Y. Moon, and S. J. Yoo, "Electron characterization in weakly ionized collisional plasmas: from principles to techniques," Adv. Phys.: X **4**(1), 1526114 (2019).
9. Y. Pan, K. Tomita, Y. Kawai, M. Matsukuma, and K. Uchino, "Measurements of spatial distributions of electron density and temperature of 450 MHz UHF plasma using laser Thomson scattering," Jpn. J. Appl. Phys. **60**(SA), SAAB03 (2021).

OPTICS CONTINUUM

10. Z. He, C. Smith, Z. Zhang, T. Biewer, N. Jiang, S. Roy, and P. Hsu, "Pulse-burst laser-based 10 kHz Thomson scattering measurements," Plasma Sci. Technol. **21**(10), 105603 (2019).
11. N. Kafle, T. M. Biewer, and D. C. Donovan, "Dual-pass upgrade to the Thomson scattering diagnostic on the Prototype-Material Plasma Exposure eXperiment (Proto-MPEX)," Rev. Sci. Instrum. **89**(10), 10C107 (2018).
12. S. Hübner, J. S. Sousa, J. van der Mullen, and W. G. Graham, "Thomson scattering on non-thermal atmospheric pressure plasma jets," Plasma Sources Sci. Technol. **24**(5), 054005 (2017).
13. A. F. H. van Gessel, E. A. D. Carbone, P. J. Bruggeman, and J. J. A. M. van der Mullen, "Laser scattering on an atmospheric pressure plasma jet: disentangling Rayleigh, Raman and Thomson scattering," Plasma Sources Sci. Technol. **21**(1), 015003 (2012).
14. R. Miles, A. Dogariu, and L. Dogariu, "Localized time accurate sampling of nonequilibrium and unsteady hypersonic flows: methods and horizons," Exp. Fluids **62**(12), 248 (2021).
15. C. V. Filip, S. Y. Tochitsky, R. Narang, C. E. Clayton, K. A. Marsh, and C. J. Joshi, "Collinear Thomson scattering diagnostic system for the detection of relativistic waves in low-density plasmas," Rev. Sci. Instrum. **74**(7), 3576–3578 (2003).
16. S. H. Glenzer, O. L. Landen, P. Neumayer, R. W. Lee, K. Widmann, S. W. Pollaine, R. J. Wallace, G. Gregori, A. Höll, T. Bornath, R. Thiele, V. Schwarz, W. D. Kraeft, and R. Redmer, "Observations of Plasmons in Warm Dense Matter," Phys. Rev. Lett. **98**(6), 065002 (2007).
17. E. Carbone and S. Nijdam, "Thomson scattering on non-equilibrium low density plasmas: Principles, practice and challenges," Plasma Phys. Control. Fusion **57**(1), 014026 (2015).
18. W. Lee, "Development of Raman and Thomson scattering diagnostics for study of energy transfer in nonequilibrium, molecular plasmas," PhD diss., The Ohio State University, (2003).
19. A. Roettgen, I. Shkurenkov, M. Simeni Simeni, I. V. Adamovich, and W. R. Lempert, "Time-resolved electron temperature and electron density measurements in a nanosecond pulse filament discharge in H_2–He and O_2–He mixtures," Plasma Sources Sci. Technol. **25**(5), 055008 (2016).
20. Naibo Jiang, Paul S. Hsu, Jason G. Mance, Yue Wu, Mark Gragston, Zhili Zhang, Joseph D. Miller, James R. Gord, and Sukesh Roy, "High-speed 2D Raman imaging at elevated pressures," Opt. Lett. **42**(18), 3678–3681 (2017).